

# **Graphene Oxide Nanoplatfoms to Enhance Catalytic Performance of Iron Phthalocyanine for Oxygen Reduction Reaction in Bioelectrochemical Systems**

Maida Aysla Costa de Oliveira<sup>a</sup>, Barbara Mecheri<sup>a\*</sup>, Alessandra D'Epifanio<sup>a</sup>, Ernesto Placidi<sup>b,c</sup>, Fabrizio Arciprete<sup>b</sup>, Federica Valentini<sup>a</sup>, Alessando Perandini<sup>d</sup>, Veronica Valentini<sup>e</sup>, and Silvia Licoccia<sup>a\*</sup>

<sup>a</sup> Department of Chemical Science and Technologies, University of Rome Tor Vergata, Via della Ricerca Scientifica, 00133 Rome, Italy.

<sup>b</sup> Department of Physics, University of Rome Tor Vergata, Via della Ricerca Scientifica, 00133 Rome, Italy.

<sup>c</sup> CNR-ISM, Via Fosso del Cavaliere 100, I-00133 Rome, Italy

<sup>d</sup> Department of Chemistry, Sapienza University of Rome, Piazzale Aldo Moro 2, 00185 Rome, Italy

<sup>e</sup> CNR-ISM, Via Salaria km 29.300, 00016 Monterotondo Scalo, Rome, Italy

\* Corresponding authors:

Dr Barbara Mecheri

phone: +39 06 7259 4488; FAX: +39 06 7259 4328

email: barbara.mecheri@uniroma2.it

Professor Silvia Licoccia

phone: +39 06 7259 4386; FAX: +39 06 7259 4328

email: licoccia@uniroma2.it

## **Abstract.**

We report the development of electrocatalysts based on iron phthalocyanine (FePc) supported on graphene oxide (GO), obtained by electrochemical oxidation of graphite in aqueous solution of LiCl, LiClO<sub>4</sub>, and NaClO<sub>4</sub>. Structure, surface chemistry, morphology, and thermal stability of the prepared materials were investigated by Fourier transform infrared spectroscopy (FTIR), Raman spectroscopy, atomic force microscopy (AFM), thermogravimetric analysis (TGA), and X-ray photoelectron spectroscopy (XPS). The catalytic activity toward oxygen reduction reaction (ORR) at neutral pH was evaluated by cyclic voltammetry. The experimental results demonstrate that the oxidation degree of GO supports affects the overall catalytic activity of FePc/GO, due to a modulation effect of the interaction between FePc and the basal plane of GO. On the basis of electrochemical, spectroscopic, and morphological investigations, FePc/GO\_LiCl was selected to be assembled at the cathode side of a microbial fuel cell prototype, demonstrating a good electrochemical performance in terms of voltage and power generation.

Keywords: Graphene Oxide; Iron phthalocyanine; Oxygen reduction reaction; Bioelectrochemical Systems.

## **1. Introduction**

Bioelectrochemical systems (BESs) can be considered as an innovative and flexible platform for integrated waste treatment and energy/resource recovery. All BESs share the same principle in the anode chamber where biodegradable substrates are oxidized by exoelectrogen bacteria during their anaerobic respiration. By diversifying the reaction at the cathode side, a great variety of applications have been developed, such as direct power generation (microbial fuel cells, MFCs), chemical

production (microbial electrolysis cells, MECs; microbial electrosynthesis cells, MESs), or water desalination (microbial desalination cells, MDCs) [1-4]. The extensive research work that has been devoted to this technology over the past decade demonstrates the promising outlook of BESs for highly efficient, energy-saving, and sustainable wastewater treatment [5-7]. On the other hand, practical application and widespread diffusion of BESs are still limited by the high costs associated to the materials used for device assembly, such as polymer separators and cathode materials [8, 9]. The slow kinetics of oxygen reduction reaction (ORR) led to the use of expensive catalysts, such as platinum, to reduce the overpotential and accelerate ORR. It is then paramount to develop non precious ORR catalysts to boost performance of microbial fuel cells and classify them as a sustainable technology. A great variety of materials has been investigated for MFC cathodes, including catalysts based on activated carbons (ACs) , metal–nitrogen–carbon (M-N-C) complexes, biocatalysts, and photoelectrocatalysts [10-13]. In particular, nitrogen-doped ACs and M-N-C catalysts allowed achieving ORR rate comparable to Pt, the morphology and structure of the catalysts playing an important role on efficiency and durability of ORR active sites [14-18].

The development of new carbon nanostructures with highly tunable morphology and structure has led to the use of graphene for several applications, including the assembly of components of MFC cathodes [19-21]. It has been demonstrated that ORR is effectively catalyzed by graphene-based materials due to high density of active sites, high electrical conductivity, and ease of functionalization [22-24].

Graphene oxide (GO), is also it a promising candidate as catalyst support. The presence of oxygen-containing surface functionalities and its hydrophilicity has a beneficial effect towards preventing the restack of graphene sheets, which leads to the decrease of anchoring sites for catalyst particles [25-26].

However, challenges, such as complexity in synthesis and high costs, still limit the applicability of graphene as cathode component of MFCs and other BESs.

Therefore, a facile and efficient approach to develop graphene-based catalysts can be considered a promising direction to achieve sustainable water/wastewater treatment and bioenergy production by BESs.

In this paper, we report a facile method for large-scale preparation of ORR catalysts based on iron phthalocyanine (FePc) supported on GO obtained by electrochemical oxidation of graphite in aqueous solutions of different inorganic salts (MX). By using atomic force microscopy and electrochemical and spectroscopic techniques, we correlated the different morphology and surface chemistry of GO\_MX supports with the catalytic activity of FePc/GO\_MX systems.

The investigation of the interactions between FePc and GO\_MX provided key insights for the development of graphene-based electrocatalysts for BES application.

## 2. Experimental

### 2.1 Materials preparation

Graphite rods (diameter 10 mm, length 100 cm, particle size 21-100  $\mu\text{m}$  and purity 99%) were purchased from Goodfellow. Carbon cloth with 30 wt.% PTFE wet-proofing was purchased by Quintech. Iron (II) phthalocyanine (FePc), Nafion perfluorinated resin solution (5 wt. % in lower aliphatic alcohols and water), and further chemicals were purchased from Aldrich.

*GO preparation.* Graphene oxide (GO) was prepared by electrochemical exfoliation of graphite. Two graphite rod electrodes ( $\varphi = 3 \text{ mm}$ ;  $L = 5 \text{ cm}$ ) were immersed in a cell containing 80 mL of 0.1 M aqueous solution in MX salt ( $M = \text{Li}^+, \text{Na}^+, \text{K}^+$ ;  $X = \text{Cl}^-, \text{ClO}_4^-$ ), applying 24 V voltage for  $6 \leq t \leq 22 \text{ h}$ . Subsequently, the powder (labelled as GO\_MX) was collected by drying the suspension in an oven at 70 °C overnight. GO\_MX was further dispersed in distilled water (DI) to 1 mg/mL and centrifuged at 8500 rpm for 1 h. The supernatant was removed and GO was dried in an oven at 70 °C overnight .

*Preparation of FePc/GO\_MX catalysts.* 0.5 g of FePc (Aldrich) were dissolved in 30 mL of methanol. 0.5 g of GO were added to the solution and the resulting mixture was stirred for 45 min. The mixture was heated in a water bath at 70 °C to evaporate methanol and the resulting powder was completely dried in an oven at 70 °C for 3 h, obtaining a product labeled as FePc/GO\_MX.

## **2.2 Materials characterizations**

*Atomic Force Microscopy (AFM).* AFM measurements were performed in air using a Veeco Multiprobe IIIa instrument. Experiments were carried out in tapping mode by using Si tips with a spring constant of about 40 N/m and a typical curvature radius on the tip of 7 nm. GO\_MX was dispersed in DI to a 0.01 mgmL<sup>-1</sup> content and deposited on Mica substrates.

*Fourier Transform Infrared Spectroscopy (FTIR).* The chemical structure of GO was analyzed by FTIR using a Fourier transform infrared spectrometer (Type FTIR100, Perkin Elmer) in transmittance mode. GO\_MX powder samples were pelleted in 150 mg of KBr using a Specac manual hydraulic press, by applying a pressure of 2 tons for 5 min. The diameter of pellets was 13 mm.

*Raman Spectroscopy.* Measurements were performed with a Raman spectrometer XY Dilor, recording the spectrum from 1200 to 2900 cm<sup>-1</sup>, with resolution of 2c m<sup>-1</sup>, using an excitation wavelength of 514.5 nm. The power of the laser beam is 3.5 mW, focused on the sample by using a 100X objective and performing 10 repetitions of 60 s, for each measurement. GO\_MX was deposited on Si(111) surface, starting from 1 mgmL<sup>-1</sup> dispersion in isopropyl alcohol treated in an ultrasonic bath for 1 h.

*X-ray Photoelectron Spectroscopy (XPS).* XPS was performed using an Omicron DAR 400 Al/Mg K $\alpha$  nonmonochromatized X-ray source, and a VG-CLAM2 electron spectrometer. GO\_MX was dispersed in ethanol to a 1 mgmL<sup>-1</sup> content and deposited on silicon wafer.

*Thermogravimetric Analysis (TGA).* Thermal Analysis was performed by using a TGA/DSC1 Star System (Mettler Toledo), in N<sub>2</sub> with a heating rate of 5 °C/min.

*Cyclic Voltammetry (CV)*. The catalytic activity towards ORR of the prepared materials was examined by cyclic voltammetry, using a VMP3 Potentiostat (Bio Logic Science Instruments) controlled by computer through EC-Lab V10.18 software. A conventional three-electrode cell was used: the reference electrode was a saturated electrode calomel-SCE, Amel 303/SCG/12), the auxiliary electrode was a platinum wire (Amel, 805/SPG/12), and the working electrode (WE) was a glassy carbon disk (GC, 0.196 cm<sup>2</sup> area) modified with catalyst layer. Prior to measurements, GC was cleaned by diamond paste, washed with DI and treated in an ultrasonic bath in isopropanol for 15 minutes. CV experiments were carried out in 100 mM neutral phosphate buffer solution, saturated in nitrogen and oxygen atmosphere at room temperature. The potential window was +0.6 V ÷ -0.9 V and the scan rate 5 mVs<sup>-1</sup>. Electrode surface electrical double-layer capacitance, C<sub>DL</sub>, of was estimated by recording CV curves in an N<sub>2</sub>-saturated atmosphere, with a scan rate range of 20–500 mVs<sup>-1</sup>, and measuring the charging current at 0.4 V, in the absence of faradic contribution.[27-29].

The catalyst layer was prepared by dispersing 0.8 mg of FePc/GO\_MX in 270 µL of DI and 135 µL of ethanol. This dispersion was treated in an ultrasonic bath for 30 min. Then, 50 µL of Nafion solution were added to the dispersion and vortexed for 2 minutes. 30 µL of the obtained dispersion were deposited on the GC electrode to a catalyst loading of 0.3 mgcm<sup>-2</sup> and dried at 70 °C for 12 min under vacuum.

### **2.3 Cathode preparation and characterization**

MFC cathodes were prepared by modifying carbon cloth electrodes with two layers: the diffusion layer (exposed to air) and the catalyst layer (faced to MFC solution). The diffusion layer was prepared as previously described [30]. The deposition of the catalyst layer was carried out on the opposite side of the diffusion layer, by brushing a suspension prepared from 0.5 mgm<sup>-2</sup> of FePc/GO\_MX catalyst in 0.83 µL DI, 6,67 µL Nafion solution, and 3.33 µL 2-propanol. The electrodes were dried at room

temperature for 24h. A standard Pt/C cathode was also prepared and used to assemble reference MFCs [31]. The metal (either iron or platinum) loading at the cathode side was  $0.5 \text{ mgcm}^{-2}$ .

#### **2.4 MFC fabrication and operation.**

The electrochemical cell consisted in a single-chamber air-cathode MFC (inner volume: 28 mL) assembled as previously reported with a graphite fiber brush as anode and the modified carbon cloth as cathode (diameter 4 cm) [32]. MFCs were firstly acclimated as described before and fed with phosphate buffer solution containing  $1 \text{ gL}^{-1}$  of sodium acetate. Polarization and power density curves were acquired by varying the external resistance ( $10\text{-}10000 \text{ }\Omega$ ) every 30 min intervals and measuring the cell voltage at each resistance. All the measurements were carried out at room temperature ( $23 \pm 3^\circ\text{C}$ ), acquiring three independent replicates for each cathode.

### 3. Results and Discussion

#### 3.1 GO characterization

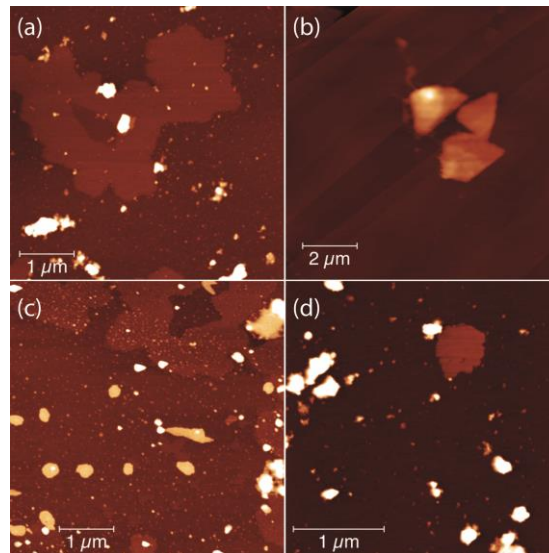


Fig. 1. AFM topographies of (a) GO\_LiCl at high magnification, (b) GO\_LiCl at low magnification, (c) GO\_LiClO<sub>4</sub>, and (d) GO\_NaClO<sub>4</sub>.

Fig. 1 shows the AFM topographies of GO<sub>MX</sub> samples. For comparable areas, analysis of several AFM images revealed significant differences for the three samples. GO\_LiCl (Fig.1a) exhibits GO sheets with surface area higher than 10 μm<sup>2</sup> and height in the range of 1-4 monolayers (ML). Moreover, we observe the presence of graphene sheets having regular edges oriented at well-defined angles (Fig 1b). Differently, graphene sheets with regular edges have not been identified for both GO\_LiClO<sub>4</sub> and GO\_NaClO<sub>4</sub>. In particular, GO sheets in GO\_LiClO<sub>4</sub> (Fig 1c) have smaller surface area (0.03-0.15 μm<sup>2</sup>) and height in the range of 3-4 ML. Nonetheless, wider GO sheets (~ 1-2 μm<sup>2</sup>) are somewhere present. In GO\_NaClO<sub>4</sub> (Fig. 1d), only some small GO sheets (0.03-0.25 μm<sup>2</sup>, in average 3-4 ML high) can be observed.

Fig. 2a shows the Raman spectra of GO<sub>MX</sub> samples and Table 1 lists the corresponding parameters. As typical fingerprint of graphene, all samples exhibit a G-band at around 1580 cm<sup>-1</sup> and a 2D-band at



2700  $\text{cm}^{-1}$ , corresponding to the first-order scattering of the E2g vibration mode and the second-order two phonon mode, respectively. Moreover, a D-band is also observed at 1350  $\text{cm}^{-1}$ , which is attributed to the disorder-induced mode due to the presence of structural defects [33].

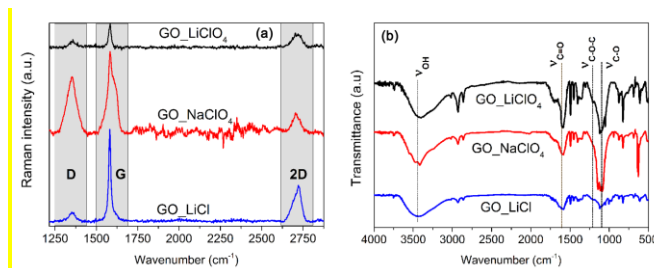


Fig. 2. Raman (a) and FTIR (b) spectra of GO\_MX samples

The intensity ratio of D and G bands ( $I_D/I_G$ ), also reported in Table 1, provides important information about the defects introduced on graphene surface and edges during the electrochemical exfoliation. Among the series of samples, GO\_LiCl has the lowest  $I_D/I_G$  ratio indicating that this sample has the lowest content of defects. This feature can be related to the regular morphology of GO\_LiCl highlighted by AFM results (Fig. 1b). The higher  $I_D/I_G$  ratio of GO\_LiClO<sub>4</sub> and GO\_NaClO<sub>4</sub> also explains the irregular shape of GO sheets, observed in the AFM micrograph shown in Fig. 1c and 1d, respectively. The correlation between the content of defects and the regularity in morphology of graphene sheets has been already observed in literature [34,35].

Information about oxygen-containing groups on the surface of GO\_MX samples are obtained by FTIR Spectroscopy (Fig. 2b). The most characteristic features of the FTIR spectra of all samples, are the bands at 1300-1000  $\text{cm}^{-1}$  (C-O stretching vibrations from carboxyl and epoxide groups), 1720-1706  $\text{cm}^{-1}$  (C=O stretching vibrations from carbonyl and carboxyl groups), and 3570-3425 (O-H stretching vibrations). Hence, all GO\_MX samples show a rich variety of transmittance bands due to carbonylic, carboxylic, epoxide, and hydroxylic groups, in good agreement with previous works [36].

X-ray photoelectron spectroscopy (XPS) further clarifies the surface composition and oxidation of graphene. The C1s spectra of GO\_LiCl, GO\_LiClO<sub>4</sub>, and GO\_NaClO<sub>4</sub> are shown in Fig. 3a, 3b, and 3c, respectively and Table 2 shows the results of the deconvolution of the relative C1s peaks. For all samples, the presence of aromatic C=C and aliphatic C-C is demonstrated by the main peak at binding energy around 284 eV. All samples also show a considerable degree of oxidation, as indicated by the presence of hydroxyl, epoxide, carbonyl, and carboxyl functional groups.  $\pi$ - $\pi^*$  peaks assigned to  $\pi$  electrons delocalized in the aromatic network are also present around 291 eV. Among the three samples, the non-oxidized carbon component is more intense for GO\_LiCl and GO\_NaClO<sub>4</sub>, while GO\_LiClO<sub>4</sub> shows the highest oxygen-containing functional groups, therefore the highest degree of oxidation.

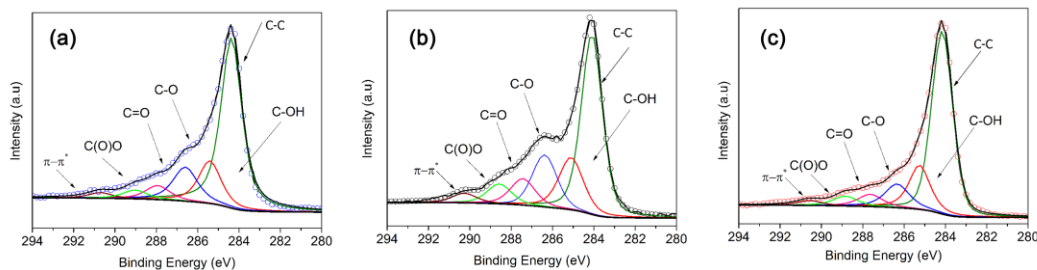


Fig. 3. C1s XPS spectra and related fit of (a) GO\_LiCl, (b) GO\_LiClO<sub>4</sub>, and (c) GO\_NaClO<sub>4</sub>.

Fig. 4 shows the TG curves and the corresponding DTG for GO\_MX samples giving information on the thermal induced desorption of oxygen-containing groups at GO\_MX surface .

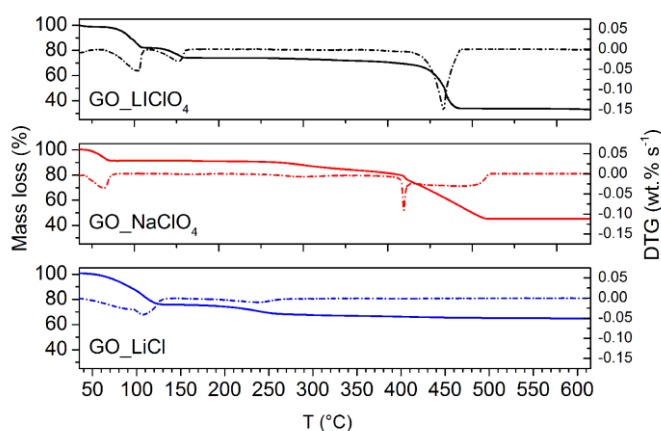


Fig. 4. Thermogravimetric (TG) and differential thermogravimetric (DTG) curves of GO\_MX samples.

The samples exhibit up to three steps of mass losses associated to the desorption of physisorbed water (mass loss I, in the 25-115 °C range), the removal of oxygen-containing groups accompanied by the splitting-off of CO<sub>x</sub> and H<sub>2</sub>O molecules (mass loss II, in the 115-400°C range), and the combustion of residual perchlorates ions (mass loss III, in the 400-550°C range, absent for GO\_LiCl sample).

Table 3 summarizes and compares the parameters obtained for all samples, such as weight loss percentage (wt.%), temperature range (T), and temperature of maximum rate of weight change (T<sub>MAX</sub>).

The main difference in the TGA/DTG profiles reside in the lowest T<sub>MAX</sub> of weight change in mass loss II for GO\_LiClO<sub>4</sub>. This can be associated to the high content of relatively unstable oxygen-containing functional groups of GO\_LiClO<sub>4</sub>, in agreement with XPS results. Despite its low oxidation degree, the amount of physisorbed water of GO\_LiCl is the highest among the GO series due to the high hygroscopicity of residual salt.

The catalytic activity towards ORR of the prepared samples was investigated by CV. While no peaks were detected under N<sub>2</sub> purging, all samples showed a reduction peak around -0.2 V, indicating catalytic activity towards ORR (Fig. S1). For the three samples, position and intensity of the peaks are

very similar (about -0.2 V and -0.2 mAcm<sup>-2</sup>, respectively), indicating that the morphology and oxidation degree of the supports have a negligible effect on ORR catalysis.

### 3.2 FePc/GO\_MX characterization

To obtain highly active catalysts towards ORR, iron phthalocyanine is supported on GO\_MX samples as described in the experimental (section 2.1). We acquired CVs of FePc/GO\_MX samples in both N<sub>2</sub>- and O<sub>2</sub> saturated electrolyte (Fig. 5). The deposition of iron phthalocyanine on GO\_MX supports results in a positive shift of the oxygen reduction potential and in an increase of peak current density with respect to GO\_MX samples. The more positive potential and the higher current density of the oxygen reduction peak indicate higher ORR activity.

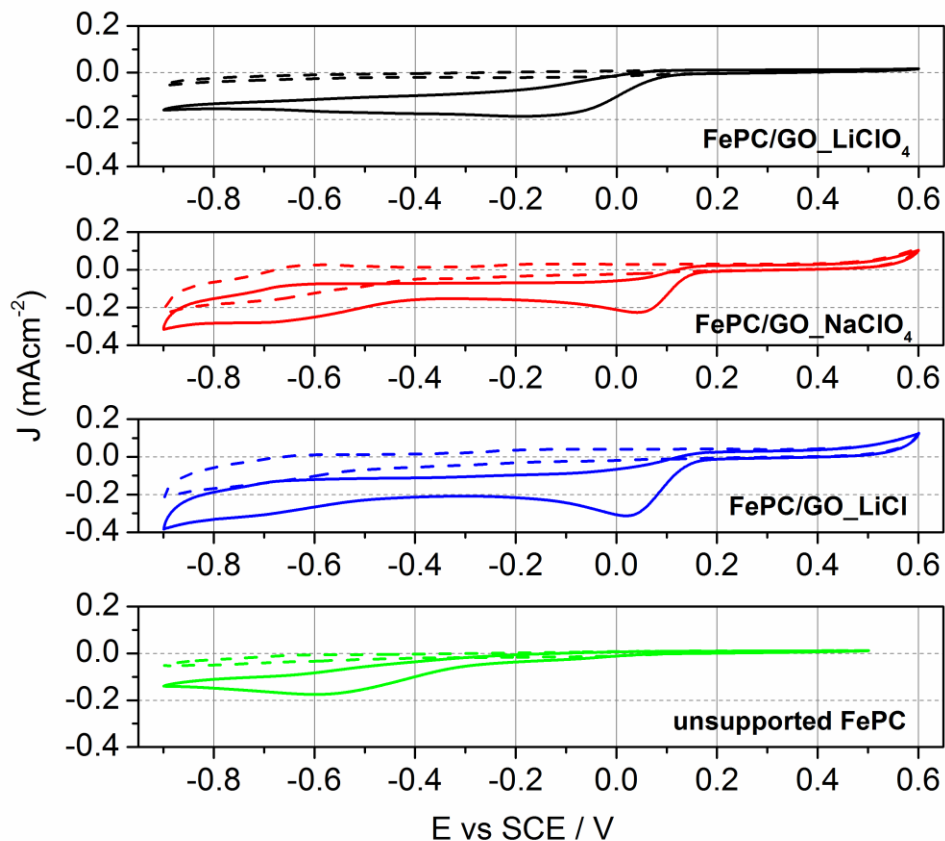


**Fig. 5.** Cyclic Voltammograms of **unsupported FePc** and FePc/GO\_MX samples in N<sub>2</sub>- (dashed lines) and O<sub>2</sub>-saturated (solid lines) phosphate buffer solution.

Table 4 lists the  $E_{pr}$  (potential of oxygen reduction peak) and  $|J_{pr}|$  (peak current density) for FePc/GO\_MX samples and unsupported FePc taken as reference.

The enhanced catalytic activity of FePc/GO\_MX samples arises from the coordination of iron, nitrogen (from FePc) and carbon (from both FePc and GO supports). As highlighted from previous works dealing with iron based catalysts supported on nanostructured carbon [17, 37], Fe-N-C moieties act as highly active catalytic sites for ORR catalyst. The poor catalytic activity of unsupported FePc can be ascribed to the overlap of catalytic sites and catalyst deactivation commonly associated with phthalocyanine aggregation [38]. The positive shift in  $E_{pr}$  and higher current density values clearly indicates that the interactions between FePc and GO\_MX supports have a beneficial effect in preventing aggregation phenomena of FePc molecules, maintaining an open macromolecular structure, hence providing a higher density of active sites which significantly enhances catalytic activity.

Among FePc/GO\_MX samples, FePc/GO\_LiClO<sub>4</sub> displays the poorest catalytic activity towards ORR.

**Such a feature can be ascribed to the high oxidation degree of GO\_LiClO<sub>4</sub> sample, indicated by XPS,** which might promote FePc aggregation.

To get deeper insight on this, we calculate the double-layer capacitance ( $C_{DL}$ ) of electrical double layer formed at the FePc/GO\_MX electrode–electrolyte interface upon application of DC voltage. The capacitance of this double layer depends on the structure and morphology of the electrode surface, and it is expected to increase with increasing the electrode surface area accessible to electrolyte ions [28, 39]. Unsupported FePc displays the lowest  $C_{DL}$  value (Table 4), indicating the lowest surface area accessible to electrolyte ions due to the above-mentioned aggregation phenomena. When FePc **is supported on GO\_MX,  $C_{DL}$  increases** in the series FePc/GO\_LiClO<sub>4</sub> « FePc/GO\_NaClO<sub>4</sub> <

FePc/GO\_LiCl indicating that the surface chemistry of the supports affects the overall electrocatalyst surface area; in particular, GO\_LiCl allows FePc to exhibit the highest surface area while GO\_LiClO<sub>4</sub> the lowest one. Hence, the good electrocatalytic activity of FePc/GO\_LiCl towards ORR can be ascribed to the fact that GO\_LiCl has low oxidation degree (indicated by XPS) and high exfoliation degree/high regularity (indicated by AFM), which guarantee a high density of active sites.

Given this promising feature, FePc/GO\_LiCl was selected to deepen the investigation and to get insights on the nature of Fe-C-N active sites.

The morphology of this sample mainly consists in single layer FePc/GO sheets with surface area higher than 1  $\mu\text{m}^2$ . The presence of FePc/GO with lower surface area and higher number of GO layers (3-4 ML) can be also observed (Fig. 6a).

Fig. 6b shows the FTIR spectra of FePc and FePc/GO\_LiCl together with that of GO\_LiCl. The spectrum of unsupported FePc shows stretching and bending vibration bands typical of metal phthalocyanines, including vibrations of nitrogen bridging atoms ( $1512\text{ cm}^{-1}$ ), stretching vibrations of isoindole ( $1434\text{ cm}^{-1}$ ) and pyrrole ( $1335\text{ cm}^{-1}$ ), and in plane C-H bending ( $1288, 1164, 1119, 1083\text{ cm}^{-1}$ ) [40,41].

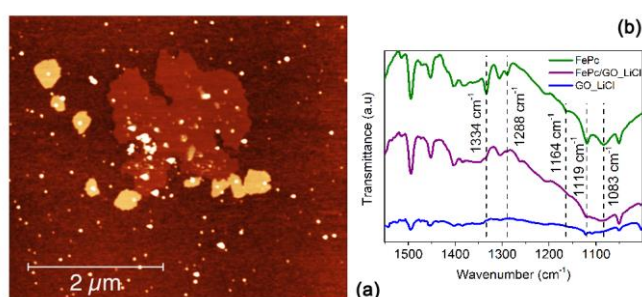


Fig 6. AFM micrograph of FePc/GO\_LiCl (a) and FTIR Spectra of FePc, FePc/GO\_LiCl, and GO\_LiCl sample (b)

When supported on GO\_LiCl, FePc shows several differences in the stretching and bending vibration bands. As highlighted by the dashed lines in Fig. 6b, the vibration band at  $1334\text{ cm}^{-1}$  disappears, while the intensities of those at  $1288$ ,  $1164$ , and  $1119\text{ cm}^{-1}$  strongly decrease, turning into a shoulder. Moreover, the band at  $1083\text{ cm}^{-1}$  becomes broader. Such differences in the FTIR spectra of FePc and FePc/GO\_LiCl can be ascribed to interactions between phthalocyanine and the basal plane of graphene via  $\pi$ - $\pi$  stacking [42].

XPS measurements were performed to get further insights on FePc/GO interaction.

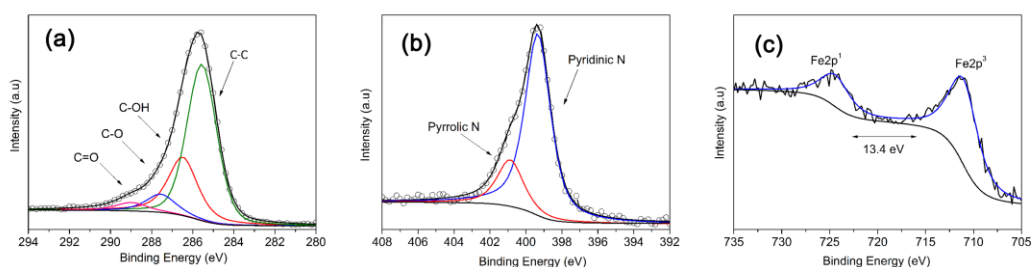


Fig. 7. XPS spectra of GO\_LiCl\_FePc (a) C1s (b) N1s, and (c) Fe2p.

Fig. 7 shows the spectra and relative fits for C, N, and Fe core peaks. The atomic percentage of unoxidized carbon in FePc/GO\_LiCl is slightly increases in comparison with that observed for GO\_LiCl (Table 5) and N 1s peak exhibits two components corresponding to pyridinic and pyrrolic nitrogen (Table 6). In nitrogen-containing carbon materials, it is believed that either pyridinic or pyrrole/pyridone type nitrogen are associated to enhanced ORR activity [17, 43,44]. The Fe 2p spectra exhibit a single component that corresponds to  $\text{Fe}^{3+}$  indicating oxidation of the metal in the composite with respect to pristine FePc. High oxidation states of a metal are known to facilitate reductive O-O cleavage [45].

### 3.3 MFC tests

Assembling of MFC prototypes equipped with FePc/GO\_LiCl as cathode allows to evaluate its electrochemical performance in terms of voltage and power generation.

Fig. 8a shows the voltage generation cycles of the cells compared with reference cells containing reference Pt/C as a function of time. MFCs assembled with Pt/C as cathode generate high and stable voltage in the first cycles (0.57 V during 350 hours), then voltage progressively decreases due to the well known Pt deactivation and poisoning in the presence of typical MFC metabolites [46]. By contrast, MFCs assembled with FePc/GO\_LiCl generate low voltage in the first cycles, but the voltage progressively increases becoming stable after ca. 350 h of operation and remaining stable and higher than that of Pt/C up to 550 h.

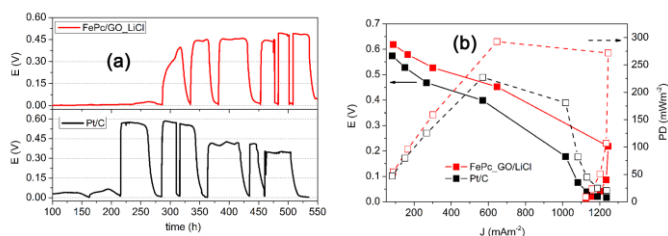


Fig. 8. (a) Voltage cycles under a 1 kV external resistance recorded for 550 h from inoculation and (b) cell voltage (E) and power density (PD) of MFCs assembled with FePc/GO\_LiCl and Pt/C cathodes and fed with 1 mgL<sup>-1</sup> sodium acetate in neutral phosphate buffer.

Polarization and power density (PD) curves of MFCs assembled with FePc/GO\_LiCl and Pt/C are acquired after 550 h from inoculation. The cell assembled with FePc/GO\_LiCl as cathode reaches a maximum power density of 295 mWm<sup>-2</sup>, corresponding to 1.2 Am<sup>-2</sup> current density. The performance is similar and even higher than that of the MFC assemble with reference Pt/C as cathode. Electricity and power generation are consistent with existing literature reporting the performance of MFCs assembled with cathodes based either on graphene or metal phthalocyanines supported on different types of nanostructured carbon [47-54].



Moreover, it should be noted that the use of nanostructured carbon as catalyst support generally implies time consuming and expensive post treatments (*i.e.*, thermal annealing and/or doping with heteroatom functionalities) to boost catalytic activity. By contrast, supporting FePc on GO\_LiCl allowed generating considerable power density, without any post treatment. This points out that FePc/GO\_LiCl has the added value of guaranteeing good performance while reducing the device costs, hence being a suitable candidate to substitute platinum as catalysts at the cathode side of bioelectrochemical systems.

#### 4. Conclusions

We reported a facile method for large-scale preparation of ORR catalysts based on iron phthalocyanine (FePc) supported on graphene oxide (GO) obtained by electrochemical oxidation of graphite in aqueous solutions of LiCl, LiClO<sub>4</sub>, and NaClO<sub>4</sub>.

The body of AFM, Raman, FTIR, XPS, and TGA results indicated that we obtained exfoliated GO sheets, decorated with carbonylic, carboxylic, epoxide, and hydroxylic surface functionalities. In particular, the exfoliation degree was more pronounced for GO\_LiCl compared to GO\_LiClO<sub>4</sub> and GO\_NaClO<sub>4</sub>. Moreover, GO\_LiClO<sub>4</sub> displayed the highest oxidation degree. The high exfoliation degree associated to a relatively low oxidation degree of GO\_LiCl resulted in very well oriented graphene sheets with regular edges, as indicated by AFM micrographs.

The GO nanosheets were used as support for FePc; AFM, and FTIR analysis demonstrated the interaction between phthalocyanine and basal plane of graphene via  $\pi$ - $\pi$  stacking. The establishment of such interactions prevents FePc aggregation, and hence affects the catalytic activity towards ORR of FePc/GO systems, as indicated by cyclic voltammetry. In particular, the good electrocatalytic activity of FePc/GO\_LiCl towards ORR was ascribed to the enhanced interaction between FePc and GO support promoted by low oxidation degree and high exfoliation degree/high regularity of GO\_LiCl which all guarantee a high density of active sites.

To demonstrate the applicability of FePc/GO\_LiCl as ORR catalysts in bioelectrochemical systems, we assembled FePc/GO\_LiCl at the cathode side of a microbial fuel cell (MFC) prototype. MFCs assembled with FePc/GO\_LiCl generated stable voltage cycles and considerable power density, at reduced costs compared to reference Pt/C cathodes.

### **Acknowledgements**

The present work was carried out with the support of the “European Union's Horizon 2020 research and innovation programme”, under H2020-FTIPilot-2015-1 (Grant Agreement n. 720367-GREENERNET) and “CNPq - Conselho Nacional de Desenvolvimento Científico e Tecnológico”, Brazil. Thanks are due to Ms. Cadia D’Ottavi (Dept of Chemical Science and Technologies, University of Rome Tor Vergata) and Mr Giuseppe Piciacchia (CNR-ISM, Monterotondo) for their valuable technical support.

## References

- [1] X. Chen, P. Liang, X. Zhang, X. Huang, Bioelectrochemical Systems-Driven Directional Ion Transport Enables Low-Energy Water Desalination, Pollutant Removal, And Resource Recovery, *Bioresource Technol.* 215 (2016) 274-284.
- [2] A. Rinaldi, B. Mecheri, V. Garavaglia, S. Licoccia, P. Di Nardo, E. Traversa, Engineering Materials And Biology To Boost Performance Of Microbial Fuel Cells: A Critical Review, *Energ. Environ. SCI.* 1 (2008) 417-429.
- [3] H. Nie, T. Zhang, M. Cui, H. Lu, D.R. Lovley, T.P Russell, Improved Cathode For High Efficient Microbial-Catalyzed Reduction In Microbial Electrosynthesis Cells, *Phys. Chem. Chem. Phys.* 15 (2013) 14290-14294.
- [4] S. Sevda, H. Yuan, Z. He, I.M. Abu-Reesh, Microbial Desalination Cells As A Versatile Technology: Functions, Optimization And Prospective, *Desalination.* 371(2015) 9-17.
- [5] A. ElMekawy, S. Srikanth, S. Bajracharya, H.M. Hegab, P.S. Nigam, A. Singh, S.V. Mohan, D.Pant, Food And Agricultural Wastes As Substrates For Bioelectrochemical System (Bes): The Synchronized Recovery Of Sustainable Energy And Waste Treatment, *Food Res. Int.* 73 (2015) 213-225.
- [6] S.M Iskander, B. Brazil, J.T. Novak, Z. He, Resource Recovery From Landfill Leachate Using Bioelectrochemical Systems: Opportunities, Challenges, And Perspectives, *Bioresource Technol.* 201(2016) 347-354.
- [7] D. Pant, A. Singh, G. Van Bogaert, S. Irving Olsen, P. Singh Nigam, L Diels, K. Vanbroekhoven, Bioelectrochemical Systems (Bes) For Sustainable Energy Production And Product Recovery From Organic Wastes And Industrial Wastewaters, *RSC Adv.* 2 (2012) 1248-1263.

- [8] S. Angioni, L. Millia, G. Bruni, C. Tealdi, P. Mustarelli, E. Quartarone, Improving The Performances Of Nafion™-Based Membranes For Microbial Fuel Cells With Silica-Based, Organically-Functionalized Mesostructured Fillers, *J Power Sources*. 334 ( 2016) 120-127.
- [9] R.A. Rozendal, H.V.M. Hamelers, K. Rabaey, J. Keller, C.J.N. Buisman, Towards Practical Implementation Of Bioelectrochemical Wastewater Treatment, *Trends. Biotechnol.* 26 (2008) 450–459.
- [10] H.Yuan, Y. Hou, I.M. Abu-Reesh, J. Chen, Z. He, Oxygen Reduction Reaction Catalysts Used In Microbial Fuel Cells For Energy-Efficient Wastewater Treatment: A Review, *Mater. Horiz.* 3 (2016) 382-401.
- [11] A. G.Campo, P. Cañizares, M. A. Rodrigo, F. J. Fernández, J. Lobato, Microbial Fuel Cell With An Algae-Assisted Cathode: A Preliminary Assessment, *J Power Sources* 242 (2013) 638-645.
- [12] J. Lobato, A. González del Campo, F. J. Fernández, P. Cañizares, M. A. Rodrigo, Lagooning microbial fuel cells: A first approach by coupling electricity-producing microorganisms and algae, *Applied Energy* 110 (2013) 220-226.
- [13] I. Gajda, J. Greenman, C. Melhuish, I. Ieropoulos, Photosynthetic cathodes for Microbial Fuel Cells, *Int. J. Hydrogen Energ.* 38 (2013) 11559-11564
- [14] W. Yang, B. E. Logan, Immobilization Of A Metal-Nitrogen-Carbon Catalyst On Activated Carbon With Enhanced Cathode Performance In Microbial Fuel Cells, *ChemSusChem*. 9 (2016) 1-8.
- [15] M.T. Nguyen, B. Mecheri, A. D'Epifanio, T.P. Sciarria, F. Adani, S. Licoccia, Iron Chelates As Low-Cost And Effective Electrocatalyst For Oxygen Reduction Reaction In Microbial Fuel Cells, *Int J Hydrogen Energ.* 39 (2014) 6462-6469.
- [16] M.T. Nguyen, B. Mecheri, A. Iannaci , A. D'Epifanio, T.P. Sciarria, F. Adani, S. Licoccia, Iron/Polyindole-Based Electrocatalysts To Enhance Oxygen Reduction In Microbial Fuel Cells, *Electrochim. Acta* 190 (2016) 388-395.

- [17] A. Iannaci, B. Mecheri, A. D'Epifanio, M. J. Lázaro Elorri, S. Licoccia, Iron–Nitrogen-Functionalized Carbon As Efficient Oxygen Reduction Reaction Electrocatalyst In Microbial Fuel Cells, *Int J Hydrogen Energ.* 41 (2016) 19637-19644.
- [18] C. Santoro, A. Serov, L. Stariha, M. Kodali, J. Gordon, S. Babanova, O. Bretschger, K. Artyushkova, P. Atanassov, Iron Based Catalysts From Novel Low-Cost Organic Precursors For Enhanced Oxygen Reduction Reaction In Neutral Media Microbial Fuel Cells, *Energ. Environ. Sci.* 9 (2016) 2346-2353.
- [19] D. Torres, J.L. Pinilla, R. Moliner, I. Suelves, On The Oxidation Degree Of Few-Layer Graphene Oxide Sheets Obtained From Chemically Oxidized Multiwall Carbon Nanotubes, *Carbon.* 81(2015) 405-417.
- [20] H. Yuan, Z. He, Graphene-Modified Electrodes For Enhancing The Performance Of Microbial Fuel, *Nanoscale.* 7 (2015) 7022-7029.
- [21] M.V. Kannan, G. Gnana kumar, Current Status, Key Challenges And Its Solutions In The Design And Development Of Graphene Based Orr Catalysts For The Microbial Fuel Cell Applications, *Biosens. Bioelectron.* 77 (2016) 1208-1220.
- [22] L. Feng, Y. Chen, L. Chen, Easy-to-Operation and Low-Temperature Synthesis of Gram-Scale Nitrogen-Doped Graphene and Its Application as Cathode Catalyst in Microbial Fuel Cells, *ACS Nano.* 5 (2011) 9611–9618.
- [23] K. Parvez, S. Yang, Y. Hernandez, A. Winter, A. Turchanin, X. Feng, K. Müllen, Nitrogen-Doped Graphene And Its Iron-Based Composite As Efficient Electrocatalysts For Oxygen Reduction Reaction, *ACS Nano.* 6 (2012) 9541-9550.
- [24] Y. Liu, H. Liu, C. Wang, S.X. Hou, N. Yang, Sustainable Energy Recovery In Wastewater Treatment By Microbial Fuel Cells: Stable Power Generation With Nitrogen-Doped Graphene Cathode, *Environ. Sci. Technol.* 47 (2013), 13889–13895.

- [25] J. Hu, Y-l. Dong, X-j. Chen, H-j. Zhang, J-m. Zheng, Q. Wang, X-g. Chen, A highly efficient catalyst: In situ growth of Au nanoparticles on graphene oxide–Fe<sub>3</sub>O<sub>4</sub> nanocomposite support, *Chem Eng J* 236 (2014) 1-8
- [26] M. Lei, Z. B. Wang, J. S. Li, H. L. Tang, W. J. Liu, Y. G. Wang, CeO<sub>2</sub> nanocubes-graphene oxide as durable and highly active catalyst support for proton exchange membrane fuel cell, *Scientific Reports* 4 (2014) 7415.
- [27] L.M Da Silva, L.A De Faria, J.F.C Boodts, Determination Of The Morphology Factor Of Oxide Layers, *Electrochim. Acta.* 47 (2001) 395-403.
- [28] B.Mecheri, A. Iannaci, A. D'Epifanio, A. Mauri, S. Licoccia, Carbon-Supported Zirconium Oxide As A Cathode For Microbial Fuel Cell Applications, *ChemPlusChem.* 81 (2016) 80-85.
- [29] V. Thirumal, A. Pandurangan, R. Jayavel, R. Ilangoan, Synthesis And Characterization Of Boron Doped Graphene Nanosheets For Supercapacitor Applications, *Synthetic Met.* 220 (2016) 524-532.
- [30] A. Iannaci, T. Pepè Sciarria, B.Mecheri, F. Adani, S. Licoccia, A. D'Epifanio, Power Generation Using A Low-Cost Sulfated Zirconium Oxide Based Cathode In Single Chamber Microbial Fuel Cells, *J Alloys Compd.* 693 (2017) 170-176.
- [31] T. Pepe Sciarria, G. Merlino, B. Scaglia, A. D'Epifanio, B. Mecheri, S. Borin, S. Licoccia, F. Adani. Electricity Generation Using White And Red Wine Lees In Air Cathode Microbial Fuel Cell, *J Power Sources.* 274 (2015) 393-399.
- [32] T.P, Sciarria, A. Tenca, A. D'Epifanio, B. Mecheri, G. Merlino, M. Barbato, S. Borin, S. Licoccia, V. Garavaglia, F. Adani, Using Olive Mill Wastewater To Improve Performance In Producing Electricity From Domestic Wastewater By Using Single-Chamber Microbial Fuel Cell, *Bioresource Technol.* 147 (2013) 246-253.
- [33] A. C. Ferrari, Raman Spectroscopy Of Graphene And Graphite: Disorder, Electron–Phonon Coupling, Doping And Nonadiabatic Effects, *Solid State Commun.*143 (2007) 47–57.

- [34] C. Casiraghi, A. Hartschuh, H. Qian, S. Piscanec, C. Georgi, A. Fasoli, K. S. Novoselov, D. M. Basko and A.C. Ferrari, Raman Spectroscopy Of Graphene Edges, *Nano Lett.* 9 (2009) 1433–1441.
- [35] S.d Eigler, F. Hof, M.E. Heim, S. Grimm, P. Müller, A. Hirsch, Statistical Raman Microscopy And Atomic Force Microscopy On Heterogeneous Graphene Obtained After Reduction Of Graphene Oxide, *J Phys. Chem. C.* 118 (2014) 7698–7704.
- [36] G. Zhao, J. Li, X. Ren, C. Chen, and X. Wang, Few-Layered Graphene Oxide Nanosheets As Superior Sorbents For Heavy Metal Ion Pollution Management, *Environ. Sci. Technol.* 45 (2011) 10454–10462.
- [37] C. Santoro, A. Serov, C.W. Narvaez Villarrubia, S. Stariha, S. Babanova, A.J. Schuler, K. Artyushkova, P. Atanassov, Double-Chamber Microbial Fuel Cell With A Non-Platinum-Group Metal Fe-N-C Cathode Catalyst, *ChemSusChem.* 8 (2015) 828-834.
- [38] M. Pirouzmand, M.M Amini, N. Safari, Immobilization Of Iron Tetrasulfophthalocyanine On Functionalized Mcm-48 And Mcm-41 Mesoporous Silicas: Catalysts For Oxidation Of Styrene, *J Colloid. Interf. Sci.* 319 (2008) 199-205.
- [39] L-H. Wang, M. Toyoda, M. Inagaki, Dependence Of Electric Double Layer Capacitance Of Activated Carbons On The Types Of Pores And Their Surface Areas, *New Carbon Mater.* 23 (2008) 111-115.
- [40] A.V. Ziminov, S.M. Ramsh, E.I. Terukov, I.N. Trapeznikova, V.V. Shamanin, T.A. Yurr, Correlation Dependences In Infrared Spectra Of Metal Phthalocyanines, *Semiconductors.* 40 (2006) 1131- 1136.
- [41] A. Monteverde Videla, L. Osmieri, M. Armandi, S. Specchia, Varying The Morphology Of Fe-N-C Electrocatalysts By Templating Iron Phthalocyanine Precursor With Different Porous Sio<sub>2</sub> To Promote The Oxygen Reduction Reaction, *Electrochim. Acta.* 177 (2015) 43-50.

- [42] C. Zhang, R. Hao, H. Yin, F. Liu, Y. Hou, Iron Phthalocyanine And Nitrogen-Doped Graphene Composite as a Novel Non-Precious Catalyst for the Oxygen Reduction Reaction, *Nanoscale*. 4 (2012) 7326- 7329.
- [43] H.C. Nagaiah, S. Kundu, M. Bron, M. Muhler, W.Schuhmann, Nitrogen-Doped Carbon Nanotubes As a Cathode Catalyst For The Oxygen Reduction Reaction in Alkaline Medium, *Electrochem. Commun.* 12 (2010) 338-341.
- [44] C. Santoro, A. Serov, R. Gokhale, S. R. Carbonell, L. Stariha, J. Gordon, K. Artyushkova, P. Atanassov, A Family Of Fe-N-C Oxygen Reduction Electrocatalysts For Microbial Fuel Cell (MFC) Application: Relationships Between Surface Chemistry And Performances, *Appl. Catal. B: Environ.* 205 (2017) 24-33.
- [45] A Mahammed, M. Kosa, D.T. Major, Z. Gross, L. Elbaz, Metalloporphyrins As Nonprecious - Metal Catalysts For Oxygen Reduction N Levy *Angew, Chem. Int. Edit.* 54 (2015) 14080-14084.
- [46] U. Schröder, J. Nießen and F. Scholz, A Generation Of Microbial Fuel Cells With Current Outputs Boosted By More Than One Order Of Magnitude *Angew, Chem. Int. Ed.* 42 (2003) 2880–2883.
- [47] Y. Ren, D. Pan, X. Li, F. Fu, Y. Zhao, X. Wang, Effect Of Polyaniline-Graphene Nanosheets Modified Cathode On The Performance Of Sediment Microbial Fuel Cell, *J Chem. Technol. Biotechnol.* 88 (2013) 1946-1950.
- [48] Y. Yuan, J. Ahmed, S. Kim, Polyaniline/Carbon Black Composite-Supported Iron Phthalocyanine As An Oxygen Reduction Catalyst For Microbial Fuel Cells. *J Power Sources* .196 (2011) 1103-1106.
- [49] Y. Yuan, B. Zhao, Y. Jeon, S. Zhong, S. Zhou, S. Kim, Iron Phthalocyanine Supported On Amino-Functionalized Multi-Walled Carbon Nanotube As An Alternative Cathodic Oxygen Catalyst In Microbial Fuel Cells, *Bioresource Technol.* 102 (2011) 5849-5854.



- [50] B. Li, X. Zhou, X., Wang, B. Liu, B. Li, Hybrid Binuclear-Cobalt-Phthalocyanine As Oxygen Reduction Reaction Catalyst In Single Chamber Microbial Fuel Cells, *J Power Sources*. 272 (2014) 320-327.
- [51] J. Ahmed, H.J. Kim, S. Kim, Embedded Cobalt Oxide Nano Particles On Carbon Could Potentially Improve Oxygen Reduction Activity Of Cobalt Phthalocyanine And Its Application In Microbial Fuel Cells, *RSC Advances*. 4 (2014) 44065-44072.
- [52] B. Li, M. Wang, X. Zhou, X.Wang, B.Liu, B. Li, Pyrolyzed Binuclear-Cobalt-Phthalocyanine As Electrocatalyst For Oxygen Reduction Reaction In Microbial Fuel Cells, *Bioresource Technol*. 193 (2015) 545-548.
- [53] M. Ghasemi, W.R.W Daud, M. Rahimnejad, M. Rezayi, A. Fatemi, Y. Jafari, M.R. Somalu, A. Manzour, Copper-Phthalocyanine And Nickel Nanoparticles As Novel Cathode Catalysts In Microbial Fuel Cells, *Int. J Hydrogen Energ*. 38 (2013) 9533-9540.
- [54] J. Ahmed, Y. Yuan, L. Zhou, S. Kim, Carbon Supported Cobalt Oxide Nanoparticles-Iron Phthalocyanine As Alternative Cathode Catalyst For Oxygen Reduction In Microbial Fuel Cells, *J Power Sources*. 208 (2012) 170-175.

## Figures captions

Fig 1. AFM topographies of (a) GO\_LiCl at high magnification, (b) GO\_LiCl at low magnification, (c) GO\_LiClO<sub>4</sub>, and (d) GO\_NaClO<sub>4</sub>.

Fig. 2. Raman (a) and FTIR (b) spectra of GO\_MX samples.

Fig. 3. C1s XPS spectra and related fit of (a) GO\_LiCl, (b) GO\_LiClO<sub>4</sub>, and (c) GO\_NaClO<sub>4</sub>.

Fig. 4. Thermogravimetric (TG) and differential thermogravimetric (DTG) curves of GO\_MX samples.

Fig. 5. Cyclic Voltammograms of unsupported FePc and FePc/GO\_MX samples in N<sub>2</sub>- (dashed lines) and O<sub>2</sub>-saturated (solid lines) phosphate buffer solution.

Fig. 6. (a) AFM micrographs of FePc/GO\_LiCl and (b) FTIR Spectra of FePc, FePc/GO\_LiCl, and GO\_LiCl samples.

Fig. 7. XPS spectra of GO\_LiCl\_FePc (a) C1s (b) N1s and (c) Fe2p.

Fig. 8. (a) Voltage cycles under a 1 kV external resistance recorded for 550 h from inoculation and (b) cell voltage (E) and power density (PD) of MFCs assembled with FePc/GO\_LiCl and Pt/C cathodes and fed with 1 mgL<sup>-1</sup> sodium acetate in neutral phosphate buffer.